Published in final edited form as:
Nucl Med Biol. 2013 May ; 40(4): 451–457. doi:10.1016/j.nucmedbio.2013.01.007.

Zirconium-89 Labeled Panitumumab: a Potential Immuno-PET Probe for HER1-Expressing Carcinomas

Sibaprasad Bhattacharyya[a,*], **Karen Kurdziel**[b], **Ling Wei**[a], **Lisa Riffle**[c], **Gurmeet Kaur**[d], **G. Craig Hill**[e], **Paula M. Jacobs**[f], **James L. Tatum**[f], **James H. Doroshow**[f], and **Joseph D. Kalen**[c]

[a]ADRD, SAIC-Frederick, Frederick National Laboratory for Cancer Research (FNLCR), MD, 21702

[b]Molecular Imaging Program, CCR, NCI, NIH, Bethesda

[c]Small Animal Imaging Program/LASP, SAIC-Frederick

[d]DCTD, FNLCR

[e]Clinical Research Directorate/CMRP, SAIC-Frederick

[f]Cancer Imaging Program, DCTD, NCI, Bethesda, MD

Abstract

Introduction—Anti-HER1 monoclonal antibody (mAb), panitumumab (Vectibix®) is a fully human mAb approved by the FDA for the treatment of epidermal growth factor receptor (EGFR, HER1)-expressing colorectal cancers. By combining the targeted specificity of panitumumab with the quantitative in vivo imaging capabilities of PET, we evaluated the potential of ^{89}Zr-DFO-panitumumab PET/CT imaging and performed non-invasive, in vivo imaging of HER1 expression and estimated human dosimetry.

Methods—Panitumumab was radiolabeled with ^{89}Zrusing a derivative of desferrioxamine (DFO-Bz-NCS) and with ^{111}In using CHX-A″ DTPA as bifunctional chelators. Comparative biodistribution/dosimetry of both radiotracers was performed in non-tumor bearing athymic nude mice (n= 2 females and n=2 males) over 1-week following i.v. injection of either using ^{89}Zr-DFO-panitumumab or ^{111}In-CHX-A″-DTPA-panitumumab. Micro-PET/CT imaging of female athymic nude mice bearing human breast cancer tumors (n=5 per tumor group) with variable HER1-expression very low (BT-474), moderate (MDA-MB-231), and very high (MDA-MB-468) was performed at over 1 week following i.v. injection of ^{89}Zr-DFO-panitumumab.

Results—Radiochemical yield and purity of ^{89}Zr-Panitumumab was > 70% and > 98% respectively with specific activity 150 ± 10 MBq/mg of panitumumab in a ~ 4 hr synthesis time. Biodistribution of ^{111}In-CHX-A″ DTPA -panitumumab and ^{89}Zr-DFO-panitumumab in athymic non-tumor bearing nude mice displayed similar percent injected dose per gram of tissue with prominent accumulation of both tracers in the lymph nodes, a known clearance mechanism of panitumumab. Also exhibited was prolonged blood pool with no evidence of targeted

*bhattacharyyas2@mail.nih.gov.

Supplementary information
Two figures SI-01 and SI-02 have been provided as supplementary materials. Figure SI-01 is the graphical representation of the correlation between biodistribution of ^{89}Zr-panitumumab and ^{111}In-panitumumab. Figure SI-02 is the graphical representation of the organ dosimetry correlation of ^{89}Zr-panitumumab and ^{111}In-panitumumab.

accumulation in any organ. Human radiation dose estimates showed similar biodistributions with estimated human effective doses of 0.578 and 0.183 mSv/MBq for ^{89}Zr-DFO-panitumumab and ^{111}In-CHX-A″-DTPA –panitumumab, respectively. Given the potential quantitative and image quality advantages of PET, imaging of tumor bearing mice was only performed using ^{89}Zr-DFO-panitumumab. Immuno-PET imaging of ^{89}Zr-DFO-panitumumab in mice bearing breast cancer xenograft tumors with variable HER1 expression showed high tumor uptake (SUV > 7) in the MDA-MB-468 high HER1-expressing mice and a strong correlation between HER1-expression level and tumor uptake (R^2= 0.857, p<0.001).

Conclusions—^{89}Zr-DFO-panitumumab can prepared with high radiochemical purity and specific activity. ^{89}Zr-DFO-panitumumab microPET/CT showed uptake corresponding to HER-1 expression. Due to poor clearance, initial dosimetry estimates suggest that only a low dose ^{89}Zr-DFO-panitumumab shows favorable human dosimetry; however due to high tumor uptake, the use of ^{89}Zr-DFO-panitumumab is expected to be clinically feasible.

Introduction

Positron emission tomography (PET) is a well-established clinical imaging modality used to non-invasively identify disease presence and extent, and to monitor the effect of treatment effects (1–4). PET imaging using a radio-labeled monoclonal antibody (immuno-PET) is a very powerful technique to improve tumor detection because it combines the high sensitivity, image spatial resolution and quantitative potential of PET with the specificity of a monoclonal antibody (mAb) (4–7). For immuno-PET, the physical half-life of a positron emitter has to be compatible with the biological half-life of a mAb to achieve optimal tumor imaging. Developing a target specific PET imaging probe is one of the challenging areas of current biomedical research.

The epidermal growth factor receptor (EGFR, erb1, HER1) is a glycoprotein belonging to subclass I of the tyrosine kinase receptor super family (8). This receptor is dysregulated in a variety of cancers, including lung, colorectal, head and neck, prostate, breast, glioma, pancreatic and ovarian cancers (9). Overexpression of this receptor is associated with disease progression and treatment resistance. The anti-HER1 mAb, panitumumab (Vectibix®) is a fully human mAb approved by the FDA for the treatment of HER1-expressing colorectal cancers (10, 11). Currently, it is being evaluated in patients with other types of HER1-expressing cancers, such as breast, lung, head and neck, renal, and ovarian tumors (12). Panitumumab binds to domain III of HER1 and is rapidly internalized, leading to downregulation of cell surface HER1. It also arrests the cell cycle and inhibits tumor growth by suppressing the production of proangiogenic factors (VEGF, IL-8) by tumor cells (13). Moreover, because it is a fully human antibody, panitumumab has minimal immunogenicity when administered intravenously.

In recent years, ^{89}Zr has emerged as a promising positron-emitting radionuclide (14–19) for diagnostic immuno-PET imaging because of its longer half-life (78.4 h), which provides a close match to the biological half-life of an intact mAb. While its positron yield (22.7%) is less than ^{18}F, the mostly widely used PET radiotracer, it is comparable to other longer lived radiometal based tracers used in human PET imaging (i.e. ^{64}Cu and ^{86}Y) and is inert in the biological system (4). Moreover, based on recent clinical trials in Europe, ^{89}Zr-labeled mAbs appear to be safe for human injection (4, 18). ^{89}Zr-immuno-PET with panitumumab as a targeting ligand may be useful as a non-invasive, in vivo, quantitative biomarker of HER1-expression that may be useful in patient selection and monitoring of HER1-targeted therapies.

Herein, we report the production of ^{89}Zr-labeled panitumumab, compare its biodistribution and human dosimetry estimates with that of ^{111}In-CHX-A″-DTPA-panitumumab, and

evaluate tumor uptake in three human breast cancer xenografts expressing different levels of HER1.

1. Materials and Methods

2.1. General

Isothiocyanatobenzyl derivative of desferrioxamine (DFO-Bz-NCS) was obtained from Macrocyclics, Inc. Clinical grade panitumumab was obtained from Amgen, Inc. Water (>18.2 MΩ.cm at 25 °C, Milli Q, Millipore, MA) was purified by passing it through a 10 cm-long column of chelex resin (Bio-Rad Laboratories). All other chemicals, unless otherwise stated, were purchased from Sigma Aldrich (St. Louis, MO). Zirconium-89 was produced at the National Institute of Health (Bethesda, MD) cyclotron facility using a 16.5 MeV proton cyclotron (PETtrace, General Electric, Fairfield, CT) by proton irradiation (beam energy; 14 MeV, current; 20 uA) (p,n) reaction (2 – 5 hrs) on yttrium-89 metal mesh (200mg, 4N purity, American Elements). Zirconium-89 was separated as ^{89}Zr-oxalate from irradiated ^{89}Y-metal mesh using 0.1 M oxalic acid solution (20). BT-474, MDA-MB-231 and MDA-MB-468 cells were obtained from the Development Therapeutics Program/ DCTD/NCI/NIH Tumor Repository (Frederick National Laboratory for Cancer Research, Frederick, MD). All cell lines were maintained in RPMI 1640 supplemented with 5% fetal bovine serum and 2 mM GlutaMAX™ (Life Technologies, Grand Island, NY). For the synthesis of the ^{111}In-CHX-A″-DTPA-panitumumab, ^{111}In was purchased from Perkin-Elmer, Waltham, MA. ^{111}In-CHX-A″-DTPA-panitumumab was prepared following the literature procedure (21).

All instruments were maintained and calibrated properly as per routine quality control methods (22). For accurate quantification of ^{89}Zr-activities, the samples were counted for 1 min on a gamma counter (Wallac Wizard 1480 3″, Perkin Elmer, Waltham, MA) using an energy window of 800 – 1000 keV for ^{89}Zr (909 keV emission). ^{89}Zr radiolabeling reactions were monitored using silica gel impregnated glass-fiber instant thin-layer chromatography (ITLC-SG) paper (Pall Corp., Port Washington, NY) and analyzed on the gamma counter (Wallac Wizard 1480 3″) and a PhosphorImager (FLA 5100R, Fujifilm, Stamford, CT). All activity measurements were performed in a dose calibrator (CRC-15R Capintec, Ramsey, NJ).

2.2. Synthesis of panitumumab-DFO conjugates

We used the p-isothiocyanatobenzyl derivative of desferrioxamine (DFO-Bz-NCS) as a bifunctional chelator for ^{89}Zr labeling to panitumumab. First, the panitumumab-DFO conjugate was prepared by mixing *p*-isothiacyanatodesferrioxamine (~3 equiv. in 200μL of DMSO) with 5 mg of panitumumab in 1 mL saline. The solution pH was adjusted to 9, using 0.1 M Na_2CO_3. Then, after 1 h incubation at 37°C, the conjugate was purified by size exclusion chromatography (Sephadex G-25 M, PD10 column, GE Healthcare; dead volume 2.5 mL, eluted with 200 μL fractions of 0.9% saline). The conjugation yield (~ 4 mg, 80%) was determined by Lowry assay (23). Isolated conjugate is very stable in saline for few weeks at 2–4°C.

The number of accessible DFO chelates conjugated to panitumumab was measured by radiometric isotope dilution assays, using a trace amount of ^{89}Zr-oxalate in non-radioactive $ZrCl_4$ (aq.) solution as the radioactive source (24, 25).

2.3. Synthesis of ^{89}Zr-DFO-panitumumab

In a typical radiolabeling reaction, the pH of the ^{89}Zr-oxalate (~ 185 MBq) was initially adjusted to 7.5–8.5 with 1.0 M Na_2CO_3 in a microcentrifuge vial. Then, after CO_2(g)

evolution ceased, DFO-panitumumab (~ 1.0 mg in 200 μL of 0.9% saline) was added along with 0.5 mL of 0.5M HEPES buffer and the reaction mixture was incubated at room temperature for 1 h. The overall pH of the reaction was 7.0–8.0. Radiochemical purity (> 85 ±5 %) was determined by radio-ITLC, using saline as a mobile phase. The ^{89}Zr-DFO-panitumumab was purified by using size exclusion chromatography (Sephadex G-25 M, PD10 column, >30 kDa, GE Healthcare location, dead volume = 2.5 mL, eluted with 0.5 mL fraction of saline). Final radiochemical purity determined by radio-ITLC after PD10 purification was found to be >98% in all preparations. In the ITLC experiment, ^{89}Zr-DFO-panitumumab remained at the baseline (R_f = 0.0), whereas ^{89}Zr (aq) ions moved with the solvent front (R_f = 1).

The stability of ^{89}Zr-DFO-panitumumab with respect to the loss of radioactivity (^{89}Zr) from the mAb was determined by incubation in human serum (~ 1.85 MBq in 0.5 mL human serum) for 5 days at 37 °C. The radiochemical purity was determined by radio-ITLC and gamma-counting.

2.4. Immunoreactivity of ^{89}Zr-DFO-panitumumab

The immunoreactivity assay was performed with MDA-MB-468 cells following the procedure described in the literature (19, 21). Serial dilution of ^{89}Zr-DFO-panitumumab (30,000 – 200,000 cpm in 50 μL of BSA/PBS) were added to 12 × 17 mm test tube containing MDA-MB-468 cells (1.1×10^6 in 50 μL of BSA/PBS). Following a 2 h incubation at 37 °C, cells were washed, pelleted, and counted in a gamma counter. The percent of binding was calculated and averaged.

2.5. Specificity of ^{89}Zr-DFO-panitumumab

Receptor specificity of the probe was determined by the in-vitro blocking studies using MDA-MB-468 cells. Two different methods were implemented to determine specificity. Approximately. 1.0×10^6 cells in 50 μL of BSA/PBS were incubated at 37 °C for 1 h with unlabeled panitumumab (10 μg in 50 μL of BSA/PBS). Then radiolabeled panitumumab (~ 100,000 cpm in 50 μL of BSA/PBS) was added and the whole mixture was incubated for 2 h at 37 °C. Cells were washed, pelleted, and counted in a gamma counter. The percentage of binding was calculated. The second method implemented 1×10^6 cells incubated (37 °C, 2 h) with radiolabeled panitumumab (~ 100,000 cpm in 50 μL of BSA/PBS) and unlabeled panitumumab (10 μg in 50 μL of BSA/PBS). As previously described, cells were washed, pelleted, and counted in a gamma counter.

2.6. Cell Culture and Determination of HER1 Expression by Western Blot Analysis

Breast cancer cells (BT-474, MDA-MB-231, and MDA-MB-468) were used to develop tumor models of different HER1 expression levels (26). All cell lines were received from the Development Therapeutics Program/DCTD/NCI/NIH Tumor Repository (Frederick National Laboratory for Cancer Research, Frederick, MD) and were grown as monolayers at 37 °C, in a humidified atmosphere of 5% CO_2 and 95% air. Cells were cultured in RPMI 1640 medium supplemented with 10% fetal bovine serum (Hyclone) and 2mM glutamine (Life Technology, Grand Island, NY). Exponentially growing cells were washed twice with ice cold PBS and lysed in cell lysis buffer [20 mM Tris-HCl (pH 7.5), 150 mM NaCl, 1%v/v Triton X-100, 1 mM EGTA, 2 mM EDTA, 1 mM sodium orthovanadate, 2.5 mM sodium PP_i, 1 mM β-glycerophosphate, 10 μg/ml leupeptin, 10 μg/ml aprotinin, 1 mM phenylmethane-sulfonyl fluoride and 1× complete protease inhibitor]. Lysates were sonicated, centrifuged to remove insoluble material and protein concentration was determined using the BCA Protein assay (Pierce, Rockford, IL). SDS-PAGE was performed resolving 20 μg protein on a 4–20% Tris-Glycine gel (Invitrogen, Life Technologies, Grand Island, NY) with subsequent transfer to a PVDF membrane (EMD-Millipore, MA). The

membranes were blocked with 5% BSA in TBST (20 mM Tris–HCl, pH 7.5, 0.9% NaCl, 0.05% Tween-20) for a minimum of 1 hour at room temperature followed by overnight incubation at 4°C with EGFR antibody (Cell Signaling Technology, Inc, Danvers, MA; 1:1000 dilution in TBST) or for 1h at RT with anti β-Actin antibody (Sigma-Aldrich, St. Louis, MO; 1:10,000 dilution in TBST). Proteins were visualized by chemiluminescence (EMD Millipore, Billerica, MA) and imaged (Kodak Image Station 4000 MM, Carestream Health, New Haven, CT). Image quantitation was performed using Carestream Molecular Imaging Software v5.0.2.30 (Carestream Health, New Haven, CT).

Analysis of the HER1 expression levels is similar to the method performed on the excised tumors at the conclusion of the PET imaging study.

2.7. Animal Studies

Animal studies were performed according to the Frederick National Laboratory for Cancer Research (Frederick, MD) Animal Care and Use Committee guidelines. Biodistribution studies were performed on non-tumor-bearing athymic nude mice (n = 2 female and n=2 male per time point) (Charles River Laboratories Inc, Frederick, MD). 2.17±0.11 MBq of ^{89}Zr-DFO-panitumumab or 5.3 ± 2 MBq of ^{111}In-CHX-A″ DTPA-panitumumab were formulated in 200 μL of 0.9% saline and administered (i.v. tail-vein injection) to each mouse. Mice were then euthanized at pre-determined time-points (24, 48, 72, 96, and 144 hour post-injection). Activity concentrations (%ID/g) were analyzed at each time point for select solid organs, integrated over time, and mouse to man organ scaling factors (27) were used to calculate the total number of disintegrations (residence time) for each respective organ. The total activity within the gut, which included the stomach and small and large bowel, were used to compute the fraction of dose eliminated by the gastrointestinal system (%ID). Due to the nominal contribution of the gastrointestinal excretion, all of the clearance was assumed to be through the urinary system. Since urinary excretion was not measured, the urinary fraction was estimated to be the whole body clearance fraction at each respective time point. The calculated organ residence times for the solid organs, bladder and gastrointestinal fractions, and implementing the dynamic bladder and ICRP GI models, were entered into OLINDA/EXM 1.1 (Version 1.1, copyright Vanderbilt University, Nashville, TN, 2007) (28) to obtain the pertinent organ human dose estimates.

PET-imaging studies were performed on xenograft breast tumor bearing athymic nude female mice (n = 5 per cell line). Breast cancer BT-474, MDA-MB-231, and MDA-MB-468 cells (1×10^7), which correspond to very low (HER1 negative), mid and high HER1 protein expression levels, were subcutaneously injected into each mouse (25). Mice were administered ^{89}Zr-DFO-panitumumab (10.18±1.24 MBq, 60–70 μg of mAb in 200 μL of 0.9% saline) via tail-vein injection when tumors reached 5 mm diameter. Animals remained conscious and were allowed free access to food and water prior to and after radiopharmaceutical injection. Animal PET-imaging experiments were conducted on an Inveon micro-PET/CT scanner (Siemens Medical Solutions USA, Inc., Knoxville, TN) at approximately 24, 48, 72, 96, and 144 hours post injection. Body temperature was maintained before and during imaging using a thermostat controlled circulating warm air imaging table. The pulmonary function was monitored during scanning and the anesthesia (1–2% isoflurane in O_2 at 1 L/min) was regulated to maintain a pulmonary rate between 50 and 90 bpm. Mice were imaged in the prone position for a 5 minute CT, used for PET attenuation correction, followed by a 30 minute PET. CT acquisition: 80 kVp, 500 μA, 200 msec per step, 120 steps covering 220 degrees. PET list-mode data were acquired using an energy window of 350–650 keV and a 3.432 ns coincidence timing window. CT images were reconstructed using a cone beam algorithm resulting in 192 × 192 matrix and PET utilized Ordered Subset Expectation Maximization (OSEM-3D) with 12 subsets and 4

iterations resulting in a 256 × 256 matrix. Images were analyzed using ASIPro software; version 6.8.0.0 (Siemens Medical Solutions USA, Knoxville, TN).

At the conclusion of the PET imaging studies (144 hr post-injection); tumors were extracted and flash-frozen for determination of the EGFR expression by Western blot analysis. Quantitation was performed using Carestream Molecular Imaging Software v5.0.2.30 (Carestream Molecular Imaging, Woodbridge, CT).

3. Results and discussions

During the course of our investigations, Nayak et al. reported initial studies on ^{89}Zr-labeled panitumumab as an immunoPET probe for colorectal cancer (19). In our current studies, we validate the use of ^{89}Zr-DFO-panitumumab as a immuno-PET probe in human breast cancer xenografts with variations in HER1 expression: BT-474 (negative control); MDA-MB-231 (moderate expression); and MDA-MB-468 (very high expression). We have additionally compared the biodistribution of ^{89}Zr-DFO-panitumumab with that of ^{111}In-DTPA-panitumumab and estimated human dosimetry.

3.1. Probe synthesis

Limited coordination chemistry on Zr(IV) indicates that this cation is very inert and has a strong preference for a particular type of chelator (4). Zr(IV) is an extremely hard acidic cation, which is the main reason for its strong preference for polyatomic hard donor chelators. Desferrioxamine (DFO) is one such chelator that can form a very stable complex with Zr(IV), using its six oxygen donors from the three oxime groups (4, 14).

In the conjugation reaction, some of the primary amines of panitumumab form a stable thiourea linkage with desferrioxamine (DFO-Bz-NCS) by reacting with the isothiocyanate group of the chelator (Figure 1). The conjugation reaction is pH-sensitive. At acidic pH, the yield is very low even after a few hours of incubation, so these reactions were performed above pH 8. The conjugation yield (80%, n = 20) was determined by Lowry assay (23). The isotopic dilution assays of the conjugate revealed that the number of accessible chelates per mAb was 1.6 ± 0.2 (n = 10). Incubation for more than 2 h did not increase the degree of chelate-labeling. However, an increase in the amount of chelate (DFO-Bz-NCS) increased the number of chelates per mAb. Because a higher number of chelates may affect the receptor binding affinity of the antibody, the number of accessible chelates per mAb was restricted in between 1–2.

Radiolabeling of DFO-panitumumab with [^{89}Zr]-oxalate was achieved at room temperature in basic medium (pH 7.0–8.0) with crude radiochemical yields (> 80%, n = 20). The radiolabeling reaction was completed within 1 h. Prolonged incubation did not increase the radiochemical yield. Maintaining the pH range (7.0–8.0) of the radiolabeling reaction is very important. At lower pH, the radiochemical yield decreases dramatically. We observed that at pH ~ 5.0, the radiochemical yield was <10%. Pure ^{89}Zr-DFO-panitumumab conjugate (Figure 1) can be isolated from the radiolabeled small molecule impurities by size exclusion chromatography. The final radiochemical yield of purified ^{89}Zr-DFO-panitumumab was >70%. The product was formulated in 0.9% saline with radiochemical purity (RCP) (determined by radio-ITLC) >98% and a specific activity of 150 ± 10 MBq/mg of panitumumab (n = 10).

Incubation of ^{89}Zr-DFO-panitumumab in human serum for 5 days at 37 °C revealed < 4% decrease in RCP. This result indicates that ^{89}Zr-DFO-panitumumab displays high kinetic stability and is suitable for further in vivo studies.

For comparative biodistribution dosimetry analysis ^{111}In-CHX-A″-DTPA-panitumumab was prepared following the literature procedure (21). Chemical purity was > 96 % and specific activity was 370–520 MBq/mg of mAb (n =10).

3.2. Immunoreactivity and Specificity of the Probe

Cell-based immunoreactivity assays were performed to ascertain the biological integrity of the ^{89}Zr-DFO-panitumumab. Immunoreactivity was expressed by the specific binding of ^{89}Zr labeled panitumumab to the MDA-MB-468 cells which was 68 ± 5 %. This result was comparable to the previously reported immunoreactivity data on radiolabeled (^{86}Y, ^{89}Zr,) panitumumab (11, 19).

In a blocking experiment, when unlabeled panitumumab was first added followed by the radiolabeled panitumumab, the radioactivity bound to the cells was only 2.0 ± 0.5 % (n = 3). When unlabeled panitumumab was included along with radiolabeled panitumumab, the radioactivity bound to the cells was only 3.5 ± 0.4 % (n = 3). These results clearly demonstrate that binding was specific.

3.3. Biodistribution Studies

To assess uptake in different organs with time, biodistribution studies were conducted in non-tumor bearing athymic nude mice over one week. The actual times of sacrifice were 21, 45, 69, 93, and 141 h post-i.v. administration. As expected for an intact radiolabeled antibody (11, 21), a high uptake of ^{89}Zr-panitumumab (Figure 2) in the blood pool was observed at 21 h, with slow clearance from blood. The whole body clearance over this time was low for both. Comparison of organ biodistribution between ^{111}In- and ^{89}Zr- labeled panitumumab (Table 1) resulted in an excellent correlation ($R^2 > 0.93$ $p<0.0009$). These biodistribution results are comparable to the published results for ^{111}In-CHX-A″-DTPA-panitumumab (21). For both of the tracers, uptake in the major organs after 93 h post injection was observed to be only 1–5 %ID/g. Table 2 provides the dose estimates, with the dose limiting organ being the heart (0.854 and 2.90 mGy/MBq) and whole body effective dose 0.83 and 0.578 mGy/MBq for ^{111}In and ^{89}Zr, respectively. Human dosimetry estimates (mGy/MBq) for the radionuclide labeled panitumumab resulted in an excellent correlation $R^2 > 0.94$ $p<0.0001$ between ^{111}In- and ^{89}Zr which is expected due to the high correlation in the %ID/g previously demonstrated. Table 2 also illustrates the higher organ dose of ^{89}Zr- than ^{111}In- labeled panitumumab, due to the higher energy and emission rates (S-Values) of ^{89}Zr.

In humans, HER1 is variably expressed in the liver, gastrointestinal tract, and skin. There is a notable absence of expression in the hematopoietic cells (29). There is a 2-phase (non-linear, followed by linear) clearance of panitumumab in humans, with a rapid primary blood clearance at lower levels of panitumumab injection via the native HER1 “sink”. At higher doses (therapeutic levels) the rapid primary clearance is followed by a slower blood clearance via the lymphatic system (30, 31). There is no significant cross-reactivity between the human antibody panitumumab and mouse HER1(29), therefore the contribution of the “HER1 sink” in humans was not accounted for in our model, as such, the mouse data only represents the slower linear lymphatic clearance. Accumulation of both tracers was seen prominently in the axillary lymph nodes at all-time points; the 90% saturation of HER1-mediated blood clearance is estimated at 11.2±1.86 g/mL (95% CI, 6.70 to 15.3 g/mL) (30). When administered at a tracer dose as proposed for imaging (<1mg/dose), the dominant clearance route is expected to be through HER1 binding, and normal lymph node uptake is not expected. This will likely reduce the dose to the heart and increase that to the liver. The differences in blood clearance are not expected to affect the whole body clearance; hence the estimated human effective doses will likely remain similar.

Despite the higher per/unit radiation dose estimates, given the higher sensitivity and superior potential quantitation of PET (compared with SPECT), we chose to pursue the ^{89}Zr labeled radiotracer and subsequent imaging studies were performed using only the PET agent.

3.4. In vitro and in vivo evaluations of HER1 expression

ImmunoPET/CT imaging of ^{89}Zr-DFO-panitumumab was performed in xenografts of cell lines of pre-defined HER1 expression: BT-474, low expression (negative control), MDA-MB-231 (+), moderate expression, and MDA-MB-468, very high (+++) HER1 expression. Confirmation studies of HER1-expression levels in these three cell lines used are shown in Figure 3.

Representative PET images performed at 96 h post-injection for the three cell-lines are presented in Figure 4. Quantification of the immuno-PET images showed that at the 96 h time point, the absolute uptake of ^{89}Zr-DFO-panitumumab was about 17 ± 2 %ID/g (n = 5) in MDA-MB-231 tumors and 29±5 %ID/g (n = 5) in MDA-MB-468 tumors (Figure 5). HER1 protein expression levels were obtained from the excised tumors at the conclusion of the 144 hr post-injection PET imaging time point resulting in a strong correlation (R^2=0.857 $p<0.001$) of the ^{89}Zr-panitumumab tumor uptake with the HER1/β-actin ratio.

For validation purposes, comparisons were performed for %ID/g between tumor (mid-level HER1 expression MDA-MB-231) bearing and non-tumor bearing (biodistribution studies) animals. The organ %ID/g were obtained from PET images for several organs and the blood component for the tumor bearing mice and compared to the %ID/g calculated from the biodistribution studies, resulting in an excellent correlation $R^2 \geq 0.98$ and p-value < 0.01. The axillary lymph nodes correlation was lower (R^2=0.77, $p<0.01$), most likely due to the biologic variability in lymphatic clearance.

Our preclinical studies with different cell lines along with recently published results (19) demonstrate that ^{89}Zr-DFO-panitumumab represents a promising radiotracer for non-invasive immuno-PET measurements of HER1 expression in vivo. High in vivo stability and long half-life of ^{89}Zr allows accurate measurement of panitumumab pharmacokinetics which cannot be achieved by using other well-studied PET isotope-(e.g., ^{64}Cu-, ^{86}Y-, etc.) mAb constructs.

4. Conclusions

^{89}Zr-DFO-panitumumab has been prepared with high radiochemical purity and specific activity. The immunoconjugate was found to be stable with respect to loss of the radioisotope in human serum. While the biodistribution showed slow clearance and physiologic uptake in the lymph nodes, when administered to humans at tracer levels, this is not expected to be a problem. Despite these limitations, immuno-PET studies revealed that ^{89}Zr-DFO-panitumumab uptake correlated strongly with HER1 expression. Given the high sensitivity of PET and the high uptake in HER1-expressing tumors, initial patient imaging with ^{89}Zr-DFO-panitumumab is planned.

Supplementary Material

Refer to Web version on PubMed Central for supplementary material.

Acknowledgments

This project has been funded in whole or in part with federal funds from the National Cancer Institute, National Institutes of Health, under Contract No. HHSN261200800001E. The content of this publication does not necessarily reflect the views or policies of the Department of Health and Human Services, nor does mention of

trade names, commercial products, or organizations imply endorsement by the U. S. Government. Authors are grateful to Dr. Lawrence Szajek of cyclotron facility at NIH Bethesda for providing ^{89}Zr-oxalate.

References

1. Stahl A, Weider H, Piert M, Wester HJ, Senekowitsch-Schmidtke R, Schwaiger M. Positron emission tomography as a tool for translational research in oncology. Mol Imaging Biol. 2004; 6:214–224. [PubMed: 15262237]
2. Welch, MJ.; Redvanly, CS. Handbook of Radiopharmaceuticals, Radiochemistry and Applications. John Wiley & Sons Ltd; Chichester: 2003.
3. Wagner HN Jr. Clinical PET: It's Time Has Come. J Nucl Med. 1991; 32:561–564. [PubMed: 1849557]
4. Bhattacharyya S, Dixit M. Metallic radionuclides in the development of diagnostic and therapeutic radiopharmaceuticals. Dalton Trans. 2011; 50:6112–6128. [PubMed: 21541393]
5. Wu AM. Antibodies and antimatter: The resurgence of immuno-PET. J Nucl Med. 2009; 50:2–5. [PubMed: 19091888]
6. Nayak TK, Brechbiel MW. Radioimmunoimaging with longer-lived positron-emitting radionuclides: potentials and challenges. Bioconjugate Chem. 2009; 20:825–841.
7. Wu AM, Olafsen T. Antibodies for molecular imaging of cancer. Cancer J. 2008; 14:191–197. [PubMed: 18536559]
8. Burgess AW. EGFR family: structure physiology signaling and therapeutic targets. Growth Factors. 2008; 26:263–274. [PubMed: 18800267]
9. Ciardiello F, Tortora G. Anti-epidermal growth factor receptor drugs in cancer therapy. Expert Opin Investig Drugs. 2002; 11:755–768.
10. Bhattacharyya, S.; Wei, L.; Riffle, L.; Hill, GC.; Tatum, JL.; Doroshow, J.; Kalen, JD. Development of ^{89}Zr-labeled panitumumab as EGFR-targeted PET imaging agent. World Molecular Imaging Congress (WMIC); 2011; San Diego, USA: p. (abstract)
11. Nayak TK, Germastani K, Baidoo KE, Milenic DE, Brechbiel MW. Preparation, biological evaluation, and pharmacokinetics of the human anti-HER1 monoclonal antibody panitumumab labeled with ^{86}Y for quantitative PET of carcinoma. J. Nucl. Med. 2010; 51:942–950.
12. Wu M, Rivkin A, Pham T. Panitumumab: human monoclonal antibody against the epidermal growth factor receptors for the treatment of metastatic colorectal cancer. Clin Ther. 2008; 30:14–30. [PubMed: 18343240]
13. Yang XD, Xia XC, Corvalan JR, Wang P, Davis CG. Development of ABX-EGF, a fully human anti-EGF receptor monoclonal antibody, for cancer therapy. Crit Rev Oncol Hematol. 2001; 38:17–23. [PubMed: 11255078]
14. Verel I, Visser GWM, Boellaard R, Stigter-van Walsum M, Snow GB, van Dongen GAMS. ^{89}Zr immuno-PET: Comprehensive procedures for the production of ^{89}Zr-labeled monoclonal antibodies. J. Nucl. Med. 2003; 44:1271–1281.
15. Holland JP, Caldas-Lopes E, Divilov V, Longo VA, Taldone T, Zatorska D, Chiosis G, Lewis JS. Measuring the pharmacodynamic effects of a novel Hsp90 inhibitor on HER2/neu expression in mice using ^{89}Zr-DFO-trastuzumab. PloS ONE. 2010; 5:e8859, 1–11. [PubMed: 20111600]
16. Perk LR, Vosjan M, Visser GWM, Budde M, Jurek P, Keifer G, van Dongen GAMS. p-Isothiocyanatobenzyl-desferrioxamine: A new bifunctional chelate for facile radiolabeling of monoclonal antibodies with zirconium-89 for immuno- imaging. Eur J Nucl Med Mol Imaging. 2009; 37:250–258. [PubMed: 19763566]
17. Perk LR, Visser OJ, Stigter-Van MW, Maria JWDV, Gerard WMV, Josée MZ, Huijgens PC, van Dongen GAMS. Preparation evaluation of ^{89}Zr-Zevalin for monitoring of ^{90}Y-Zevalin biodistribution with positron emission tomography. Eur J Nucl Med Mol Imaging. 2006; 33:1337–1345. [PubMed: 16832633]
18. Börjesson PKE, Jauw YWS, Boellaard R, de Bree R, Comans EFI, Roos JC, Castelijns JA, Vosjan MJWD, Kummer JA, Leemans CR, Lammertsma AA, van Dongen GAMS. Performance of Immuno Positron Emission Tomography with Zirconium-89 labeled chimeric monoclonal

antibody U36 in the detection of lymph node metastases in head and neck cancer patients. Clin Cancer Res. 2006; 12:2133. [PubMed: 16609026]

19. Nayak TK, Germestani K, Milenic DE, Brechbiel MW. PET and MRI of metastatic peritoneal and pulmonary colorectal cancer in mice with human epidermal growth factor receptor 1-targeted ^{89}Zr-labeled panitumumab. J Nucl Med. 2012; 53(1):113–120. [PubMed: 22213822]
20. Holland JP, Sheh Y, Lewis J. Standardized method for the production of high specific activity zirconium-89. Nucl Med Biol. 2009; 36:729–739. [PubMed: 19720285]
21. Ray GL, Baidoo KE, Wong KJ, Williams M, Germastani K, Brechbiel MW, Milenic DE. Preclinical evaluation of a monoclonal antibody targeting the epidermal growth factor receptor as a radioimmunodiagnostic and radioimmunotherapeutic agent. British J of Pharm. 2009; 157:1541–1548.
22. Zanzonico P. Routine quality control of clinical nuclear medicine instrumentation: a brief review. J Nucl Med. 2009; 49:1114–1131. [PubMed: 18587088]
23. Lowry OH, Rosebrough NJ, Farr AL, Randall RJ. Protein measurement with the folin phenol reagent. J Biol Chem. 1951; 193:265–275. [PubMed: 14907713]
24. Meares CF, McCall MJ, Reardan DT, Goodwin DA, Diamanti CI, McTigue M. Conjugation of antibodies with bifunctional chelating agents: isothiocyanate and bromoacetamide reagents, methods of analysis, and subsequent addition of metal ions. Anal Biochem. 1984; 142:68–78. [PubMed: 6440451]
25. Bhattacharyya, S.; Cheal, SM.; Hill, GC.; Griffiths, GL. Radiometric metal binding assay to determine chelate to protein ratio: a comparative study between ^{57}Co and ^{111}. Am. Chem. Soc. Meeting; 2009; Washington DC. p. (abstract)
26. Konecny GE, Pegram MD, Venkatesan N, Finn R, Yang G, Rahmeh M, Untch, Rusnak MD, Spehar WG, Mullin RJ, Keith BR, Gilmer TM, Berger M, Podratz KC, Slamon DJ. Activity of the Dual Kinase Inhibitor Lapatinib (GW572016) against HER-2-Overexpressing and Trastuzumab-Treated Breast Cancer. Cells Cancer Res. 2006; 66(3):1630.
27. Stabin, MG. Fundamentals of Nuclear Medicine Dosimetry. Springer; 2008.
28. Stabin MG, Sparks RB, Crowe E. OLINDA/EXM: The Second-Generation Personal Computer Software for Internal Dose Assessment in Nuclear Medicine. J Nucl Med. 2005; 46:1023–1027. [PubMed: 15937315]
29. Cohenuram M, Saif MW. Panitumumab the first fully human monoclonal antibody: from the bench to the clinic. Anticancer Drugs. Jan; 2007 18(1):7–15. [PubMed: 17159497]
30. Rowinsky EK, Schwartz GH, Gollob JA, et al. Safety, pharmacokinetics, and activity of ABX-EGF, a fully human anti-epidermal growth factor receptor monoclonal antibody in patients with metastatic renal cell cancer. J Clin Oncol. Aug 1; 2004 22(15):3003–3015. [PubMed: 15210739]
31. Foon KA, Yang XD, Weiner LM, et al. Preclinical and clinical evaluations of ABX-EGF, a fully human anti-epidermal growth factor receptor antibody. Int J Radiat Oncol Biol Phys. Mar 1; 2004 58(3):984–990. [PubMed: 14967460]

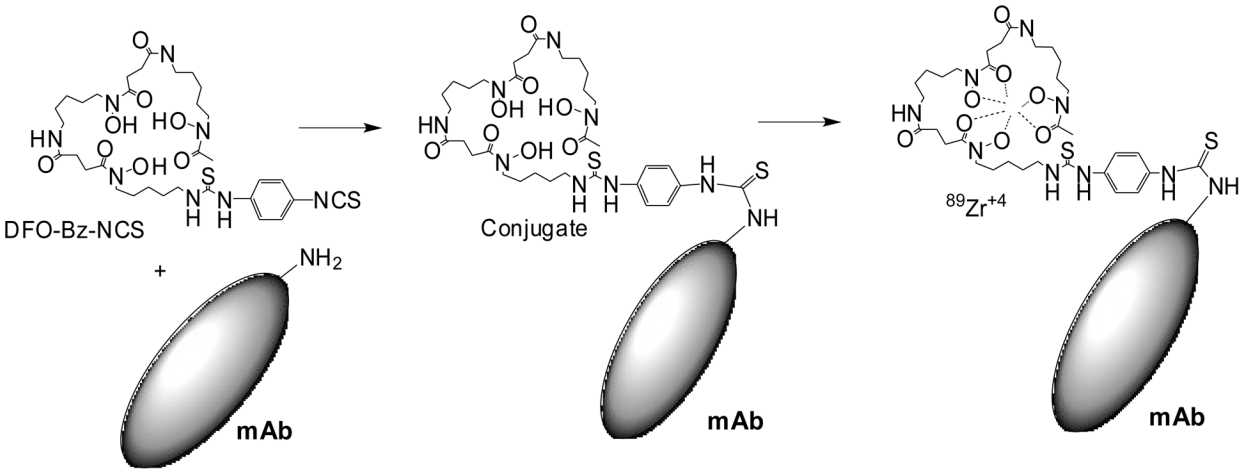

Figure 1.

Schematic representation of DFO panitumumab (mAb) conjugation reaction and radiolabeling of DFO-panitumumab conjugate with ^{89}Zr. At basic pH, isothiocyanate group of DFO react with primary amine functionality of mAb to form a stable thiourea linkage. ^{89}Zr-oxalate is used to make stable ^{89}Zr-DFO-panitumumab complex at room temperature.

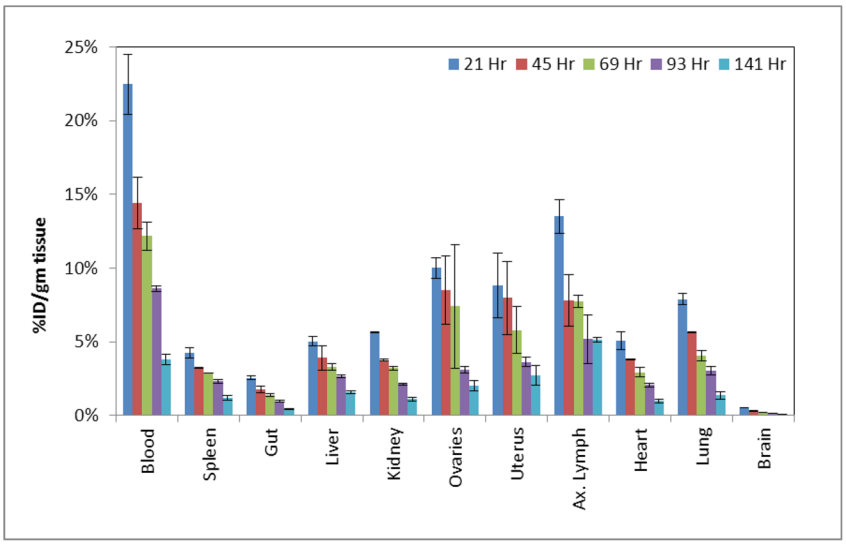

Figure 2.
Biodistribution (%ID/gm) of [^{89}Zr]Zr-panitumumab in non-tumor bearing female athymic nude mice; n = 4 per time point following i.v. administration.

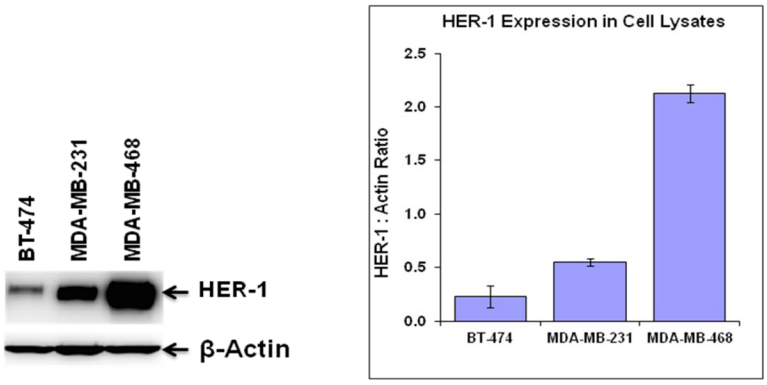

A B

Figure 3.

Comparative EGFR expression level of BT-474, MDA-MB-231, and MDA-MB-468 cell lines by western blot analysis (A). Quantitation of each band was performed using Carestream Molecular Imaging Software v5.0.2.30 and data is presented as HER-1/Actin ratio from six blots (B). Data expressed as the mean of the values ± the standard deviation.

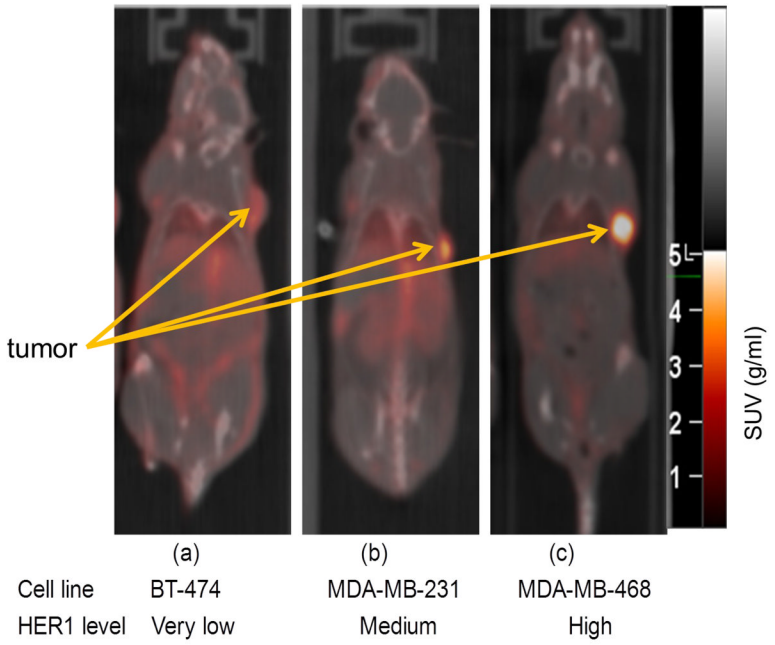

Figure 4.

Tumor uptake of ^{89}Zr-panitumumab in various subcutaneous athymic nude female xenograft models; 10.18±1.24 MBq of ^{89}Zr-panitumumab were administered intravenously via tail-vein, and a 5 min CT scan followed by a 30 min static PET scan were performed at 96 h post-injection.

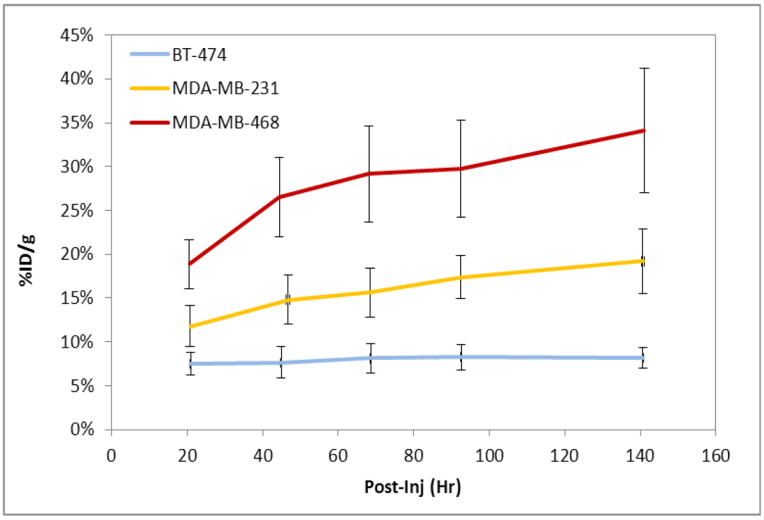

Figure 5.

Tumor time-activity curve (decay corrected) of the ^{89}Zr-panitumumab immuno-PET images of tumor (BT-474, MDA-MB-231, and MDA-MB-468) bearing athymic nude female mice (n =5 per tumor model). Mice were i.v. injected (10.18±1.24 MBq) via tail-vein. Analyses of the immuno-PET images of female athymic mice (n =5).

Table 1

Biodistribution %ID/g (average ± standard dev) comparison in female non-tumor bearing athymic nude mice (n = 2) at 21 and 90 hr post injection for radionuclide(s) ^{111}In- and ^{89}Zr- labeled panitumumab. Mice were i.v. injected 1.85 MBq and 5.3 MBq via tail-vein for ^{89}Zr-panitumumab and ^{111}In-panitumumab, respectively. The %ID/g uptake of pantimumab resulted in a good correlation $R^2 > 0.93$ $p<0.0009$ between ^{111}In- and ^{89}Zr-labeled panitumumab.

	21 hr		90 hr	
Blood/Tissues	**[^{89}Zr]Panitumumab**	**[^{111}In]Panitumumab**	**[^{89}Zr]Panitumumab**	**[^{111}In]Panitumumab**
Blood	22.47 ± 2.01	18.74 ± 5.23	8.62 ± 0.20	6.26 ± 0.24
Spleen	4.26 ± 0.37	3.79 ± 1.19	2.32 ± 0.12	1.70 ± 0.06
Gut	2.56 ± 0.13	1.92 ± 0.33	0.98 ± 0.05	0.68 ± 0.10
Liver	5.04 ± 0.31	5.04 ± 0.49	2.68 ± 0.09	2.01 ± 0.08
Kidney	5.67 ± 0.05	5.09 ± 0.84	2.13 ± 0.04	1.99 ± 0.01
Ovaries	10.01 ± 0.69	7.99 ± 0.76	3.11 ± 0.19	2.35 ± 0.01
Uterus	8.83 ± 2.21	4.40 ± 2.10	3.63 ± 0.31	2.52 ± 0.15
Ax. Lymph	13.51 ± 1.12	4.72 ± 0.33	5.19 ± 1.66	3.58 ± 0.13
Heart	5.09 ± 0.61	4.39 ± 1.10	2.08 ± 0.12	1.57 ± 0.25
Lung	7.91 ± 0.38	5.42 ± 0.20	3.04 ± 0.28	1.87 ± 0.01
Brain	0.53 ± 0.01	0.34 ± 0.10	0.15 ± 0.00	0.11 ± 0.00

Table 2

Human dosimetry (mGy/MBq) comparison for radionuclide(s) ^{111}In- and ^{89}Zr- labeled panitumumab.

	^{111}In-pan	^{89}Zr-pan
Target Organ	**mGy/MBq**	**mGy/MBq**
Adrenals	0.182	0.599
Brain	0.048	0.212
Breasts	0.112	0.391
Gallbladder	0.164	0.522
LLI	0.170	0.711
Small	0.116	0.480
Stomach	0.127	0.460
ULI	0.138	0.549
Heart	0.854	2.900
Kidneys	0.149	0.541
Liver	0.297	0.723
Lungs	0.533	0.953
Muscle	0.109	0.402
Ovaries	0.115	0.476
Pancreas	0.174	0.578
Red Marrow	0.175	0.816
Osteogenic	0.214	0.677
Skin	0.056	0.243
Spleen	0.213	0.725
Testes	0.067	0.293
Thymus	0.223	0.737
Thyroid	0.093	0.353
Urinary Bladder	0.096	0.418
Uterus	0.105	0.435
Total	0.123	0.434
Effective Dose Equivalent (mSv/MBq)	0.246	0.769
Effective Dose (mSv/MBq)	**0.183**	**0.578**